NASA TECHNICAL MEMORANDUM

NASA TM X-3517

NASA TM X-3517

ION-BEAM TECHNOLOGY AND APPLICATIONS

Wayne R. Hudson, Ronald R. Robson, and James S. Sovey

Lewis Research Center
Cleveland, Ohio 44135

NATIONAL AERONAUTICS AND SPACE ADMINISTRATION • WASHINGTON, D. C. • MAY 1977

1. Report No.	2. Government Accession No.	3. Recipient's Catalog No.
NASA TM X-3517		

4. Title and Subtitle	5. Report Date
ION-BEAM TECHNOLOGY AND APPLICATIONS	May 1977
	6. Performing Organization Code

7. Author(s)	8. Performing Organization Report No.
Wayne R. Hudson, Ronald R. Robson, and James S. Sovey	E-8910
	10. Work Unit No.
9. Performing Organization Name and Address	506-22
Lewis Research Center National Aeronautics and Space Administration Cleveland, Ohio 44135	11. Contract or Grant No.
	13. Type of Report and Period Covered
12. Sponsoring Agency Name and Address	Technical Memorandum
National Aeronautics and Space Administration Washington, D.C. 20546	14. Sponsoring Agency Code

15. Supplementary Notes

16. Abstract

Ion propulsion research and development yields a mature technology that is transferable to a wide range of nonpropulsive applications, including terrestrial and space manufacturing. In this work a xenon ion source was used for an investigation into potential ion-beam applications. The objectives of the Lewis argon-source-development program are discussed; the results of cathode tests and discharge-chamber experiments are presented. A series of experiments encompassing a wide range of potential applications is discussed. Two types of processes, sputter deposition and erosion, were studied. Some of the potential applications are thin-film Teflon capacitor fabrication, lubrication applications, ion-beam cleaning and polishing, and surface texturing.

17. Key Words (Suggested by Author(s))	18. Distribution Statement
Sputtering Ion beams Atomic physics	Unclassified - unlimited STAR Category 23

19. Security Classif. (of this report)	20. Security Classif. (of this page)	21. No. of Pages	22. Price*
Unclassified	Unclassified	36	A03

* For sale by the National Technical Information Service, Springfield, Virginia 22161

ION-BEAM TECHNOLOGY AND APPLICATIONS

by Wayne R. Hudson, Ronald R. Robson, and James S. Sovey

Lewis Research Center

SUMMARY

Ion propulsion research and development yields a mature technology that is transferable to a wide range of nonpropulsive applications, including terrestrial and space manufacturing. In this work a xenon ion source was used for an investigation into potential ion-beam applications. The objectives of the Lewis argon-source-development program are discussed; the results of cathode tests and discharge-chamber experiments are presented. A series of experiments encompassing a wide range of potential applications is discussed. Two types of processes, sputter deposition and erosion, were studied. Some of the potential applications are thin-film Teflon capacitor fabrication, lubrication applications, ion-beam cleaning and polishing, and surface texturing.

INTRODUCTION

For over 16 years the Lewis Research Center has been engaged in the research and development of electron-bombardment thrusters (ref. 1). During this period, two Space Electric Rocket Tests, SERT's I and II, have been test flown: SERT I, launched in 1964 on a 50-minute ballistic trajectory, demonstrated space ion-thruster operation and beam neutralization (ref. 2); SERT II, in 1970, demonstrated long-term (5 month) operation in space (refs. 3 and 4). This spacecraft is still operational and tests are continuing (ref. 5).

Recent efforts have been focused on demonstrating the readiness of ion-thruster systems for flight application (refs. 6 and 7). During the course of these efforts, thrusters have demonstrated lifetimes of 15 000 hours (refs. 8 and 9). Extensive testing of thruster components has also been performed. Ion-thruster hollow cathodes have been operated for more than 20 000 hours (ref. 10). A result of this propulsion research is a mature technology that is transferable to a wide range of nonpropulsive applications, including terrestrial and space manufacturing. Three generic industrial

applications have been explored, ion-beam sputter deposition, machining, and surface texturing. These applications will be discussed later.

Ion-beam sources, similar to the Lewis-electron bombardment thruster, are commercially available (refs. 11 and 12). These sources are commonly used for cleaning silicon substrates for integrated circuit fabrication and for ion-milling photoresist patterns in the fabrication of microelectronic, microwave-acoustic, and integrated-optics components (ref. 13). Similarly, high-density, microstructural arrays of Permalloy magnetic dipoles have been ion-milled for magnetic bubble devices (ref. 14). Greater resolution can be achieved with ion-milling than with chemical etching. Patterns with line widths of 1000 Å have been achieved, and the contamination that often results from chemical etching is avoided. Other applications include cleaning surfaces for surface-science research (ref. 15), polishing copper surfaces for laser mirrors (ref. 16), and producing aspheric lenses (ref. 17).

The relative positions of source, target, and substrate can be varied independently, allowing optimum etching or deposition rates. The angle of incidence of the ion beam with respect to the surface of the target is also an independent variable. Since the sputtering yield of all materials is a function of the angle of incidence and since the maximum yield occurs near 45°, the deposition rate can be maximized. In certain applications it is also desirable to etch materials at specific incidence angles. In ion-beam sputter deposition the substrate can be located outside the plasma and its temperature can be controlled. The vacuum facility pressure is also an independent variable, allowing operation at high vacuum to minimize contamination or in a controlled atmosphere for reactive sputtering.

There are several areas where thruster technology is directly transferable to industrial ion-beam sources. Research on a cusp-field-geometry thruster have shown its ability to produce very uniform beam profiles near the ion source at comparable propellant utilizations (ref. 18). More recently, the multipole concept has been shown to yield uniform current density beams for xenon and argon sources (ref. 19).

Cathodes are another area of source technology where thruster research and development results can be applied. The early electron-bombardment thrusters used various types of thermionic emitter-filaments, ribbons, and impregnated tungsten. Later emitters were replaced by hollow cathodes, primarily because of their longer operational life and reduced operating power (ref. 20). Several hollow cathodes have been operated for more than 10 000 hours and one for more than 20 000 hours (ref. 10).

Over the past decade Lewis has extensively researched large diameter thrusters, and the resulting technology may be applicable in areas such as solar-energy coatings where large work pieces are common and high production volume are required. A 30-centimeter-diameter thruster operates at a beam current of 2 amperes. The electron-bombardment ion sources are capable of parametric control. The beam current can be

smoothly varied over the complete range of operation, and the beam energy can be adjusted by changing voltage on the extraction grids. The ion beam can also be completely neutralized using a hollow cathode to supply electrons.

ION SOURCES

The experiments described in this report were performed with an 8-centimeter-diameter electron-bombardment thruster that was adapted to operate as a xenon ion-beam source. An argon source is now being developed specifically for nonpropulsive applications.

The xenon source (fig. 1) produces an 8-centimeter-diameter beam. Both the main cathode and the neutralizer are enclosed hollow cathodes with barium oxide impregnated, porous-tungsten inserts. The main cathode has a 0.635-centimeter-diameter body, a 1.27-centimeter tip-to-keeper spacing, and a 0.30-centimeter-diameter keeper orifice. The neutralizer cathode has a 0.313-centimeter-diameter body, a 1.27-centimeter tip-to-keeper spacing, and a 0.30-centimeter-diameter keeper orifice. Initially, the magnetic circuit was a SERT II divergent-field configuration (ref. 21). Later, it was modified to a cusp-field geometry. (The two configurations are compared in a later section.) The maximum magnetic field along the axis of the discharge chamber is 6.0×10^{-5} tesla. The discharge chamber has a screen anode. The beam extraction system is a dished, double-grid system. The grids are hydroformed molybdenum, dished to a depth of 0.25 centimeter. The screen grid holes are a hexagonal array of 0.19 centimeter diameter, centered 0.22 centimeter apart. The accelerator-grid hole diameters range from 0.13 centimeter in the center of the grid to 0.065 centimeter at the outer perimeter (fig. 2). The grid to grid gap is 0.635 millimeter.

Figure 3 shows the ion-source vacuum facility. The xenon source is mounted on a flange, which in turn mounts onto one of the ports of a large 1.5-meter-diameter, 4.5-meter-long vacuum facility. The port can be isolated from the facility by a 0.91-meter gate valve. The xenon source is mounted on tracks so that it can be moved as shown in figure 3. Sputtering targets are mounted on a "shepherd's crook" and can be moved as shown in figure 3. The targets can be mounted at any angle, but for sputter-deposition applications an angle of 45° was chosen for maximum sputtering rate. Several targets can be mounted and interchanged by rotating the target support. Substrates are introduced from a side port through a 10.16-centimeter-diameter gate valve. Samples can be removed (for inspection or changing) after sputter deposition without turning off the xenon source. The side port can also be used to introduce a quartz-crystal microbalance into the chamber to measure deposition rates. The substrate is supported by a rod which translates along a line perpendicular to the axis of the thruster.

The capability of independently positioning the source, target, and substrate provides flexibility to optimize sputter etching and deposition processes. For example, it is possible to move the target far downstream and rotate it so that it is completely out of the beam. Next, the substrate can be rotated and positioned so that it faces the source, where it can then be sputter cleaned by the ion beam. Then the target can be repositioned and the substrate rotated and repositioned so that deposition onto the sputter-cleaned surface begins instantaneously. Opposite the side port are viewing ports that allow the substrate and target to be illuminated and viewed at any time. The viewing ports are of additional value where the substrates are heated, in that temperature measurements can be made by optical pyrometry.

The xenon source is capable of operation at beam currents ranging from 10 to 200 milliamperes. Figure 4 is a circuit diagram of the xenon source. The net accelerating potential V_I can be varied from 500 to 2000 volts. A negative voltage V_A ranging from -200 to -500 volts is applied to the accelerator grid. This voltage prevents electrons from backstreaming into the discharge chamber and resulting in an erroneous beam-current measurement. Optimum performance is achieved when the net accelerating potential is four or five times greater than the voltage applied to the accelerator grid.

There is a 4-microfarad capacitor between the screen and the accelerator grids. During operation it is charged, and, if anything shorts the grids, the capacitor discharges, thereby clearing the short.

The capability of independently varying the net accelerating voltage and the beam current is very convenient. For certain materials such as polymers or plastics, it is desirable to reduce the beam energy and beam current to prevent damaging the target by overheating. For example, lower beam energies and currents minimize the disassociation of the polymer chains. On the other hand, higher beam current and beam energy are desirable for sputter deposition and cleaning of metals, semiconductors, and ceramics. Table I shows the range of source operating parameters. The ion-beam current as a function of total voltage of the xenon source is shown in figure 5.

Argon Source Development

Concurrent with the ion-beam applications program using the xenon source is a utilitarian argon source development. The choice of argon is dictated primarily by cost. Xenon is currently approximately 240 times more expensive than argon. The present xenon source gas operating cost averages about $1.25 per hour.

The argon source design criteria were to develop a source that is easily operated, durable, and simple to maintain. A useful source for general application should not require an expert operator. The electronic power supplies should have a minimum of controls and require a minimum of adjustment. One source design may not satisfy all

potential users. For a sputter cleaning application, a user might desire single-point operation with the minimum of controls. By way of contrast, a user who is primarily interested in sputter deposition will want to vary the beam energy. Two specific areas have been concentrated on in the development of an argon source: the cathodes and the discharge chamber. Basic types of cathodes are thermionic emitters and glow-discharge hollow cathodes. The primary advantage of the emitter cathode is its simplicity and ease of operation. Emitters have relatively short (10 hr) lives and are subject to performance degradations during operation. Hollow cathodes are longer lived, are more stable performance, and operate at lower power. Hollow cathodes have the disadvantage of being more difficult to fabricate and require a current-controlled power supply.

Cathodes

Thermionic emitters. - Three different types of emitters are under investigation: tantalum-wire filaments, oxide-coated, tantalum-ribbon filaments, and impregnated, porous-tungsten emitters. A 0.5-millimeter-diameter tantalum-wire filament was tested. A filament current of 28 amperes was required to light an argon discharge. The filament reached a temperature of 1530° C. The discharge was emission limited to 1 ampere.

An impregnated porous-tungsten emitter is shown in figure 6. It consists of a thermally isolated, impregnated porous-tungsten tube. The impregnate is an emissive mix with the mole ratio of 4 parts barium oxide, 1 part calcium oxide, and 1 part aluminum oxide. The tube is heated by a swaged heater wrapped around its outer diameter. Either xenon or argon gas is fed through the impregnated tube. When the cathode is heated to approximately 1100° C a glow discharge ignites in the tube. This particular type of emitter promises to have much longer operational life, more constant operating characteristics, and less susceptibility to poisoning when exposed to air.

Hollow cathodes. - The mercury-vapor hollow cathodes developed for the electron-bombardment thruster program were used in the xenon source development. Stable operation with xenon has surpassed 250 hours. The cathode failures encountered so far are a result of oxidation of the cathode tube and insert. The oxidation process has caused disintegration of the inserts and embrittlement of the tubes. In several cases the tubes have actually cracked. Care is required in the initial pump down and heat up after exposure to air in order to minimize the residual oxygen in the feed lines.

Figure 7 is a sketch of the cathode configuration in use. A swaged heater is wrapped around the 0.32-centimeter-diameter cathode tube and 10 layers of 1.25×10^{-3}-centimeter tantalum radiation shielding is wrapped around the heater. The cathode tip is enclosed by an aluminum oxide tube, which also establishes the spacing between the cathode tip

and the keeper electrode. The tip-to-keeper spacing was 0.25 centimeter. The cathode tip orifice is 0.025 centimeter, and the keeper orifice is 0.30 centimeter.

A parametric study of xenon and argon hollow cathodes suggests that the characteristics of a xenon hollow cathode are similar to mercury hollow cathodes. Although both types of hollow cathodes will operate over a wide range of parametric variation, the optimum values of keeper-to-tip spacing and keeper diameter are comparable. The operation of hollow cathodes on argon is more complex and characterization of operation is not complete.

The main cathode of the xenon source requires 40 watts of tip heat and a gas flow of 3 standard cubic centimeters per minute to ignite the cathode discharge. After ignition a heater power of 15 watts and a gas flow of 2 standard cubic centimeters per minute is sufficient to maintain a stable discharge. Similar operating characteristics were required for the neutralizer. Starting and operating characteristics were improved by using 0.32-centimeter-diameter cathodes rather than 0.69-centimeter diameter. Impregnated porous tungsten inserts are more durable (than the rolled-foil type developed for the SERT II thruster) at the high temperature required to start the gas cathodes.

Discharge Chamber

A second area of the argon source development is the discharge-chamber configuration. Variations in the magnetic circuit and the propellant feed have been studied. One of the most pertinent parameters is the uniformity of the ion beam. A beam with a very uniform current density over a usable diameter is particularly advantageous for sputter etching and milling applications. The beam density profile was measured with a 1.4-centimeter-diameter molybdenum button probe (biased at 15 V), which was placed 5 centimeters downstream of the source.

In an attempt to improve on the flatness of the beam profile, a magnetic circuit called the cusp-field geometry has been used (ref. 18). Figure 8 shows a cross section of this geometry. The main differences between this geometry and the SERT II geometry are the inclusion of an intermediate magnetic pole piece and use of front and back anodes. The intermediate pole piece confines the magnetic field to the outer circumference of the source resulting in a more uniform magnetic field throughout the discharge chamber. The back anode is intended to create an electric field which will spread out the electrons emitted from the cathode, thus resulting in a more uniform ion distribution. Reference 18 shows that at a beam current of 500 milliamperes the cusp field geometry produces a more uniform ion beam than does the 15-centimeter-diameter SERT II source. Figure 9 shows beam profiles measured for the xenon source with both a cusp field and the SERT II discharge-chamber geometry in an 8-centimeter-diameter source. Comparing the cusp-field beam profile with SERT II beam profile at a 100-milliampere beam

current reveals that both are relatively constant over 2 centimeters in the center of the beam. Furthermore, over a 4-centimeter diameter, both profiles are constant to within 10 percent. In both cases, the beam current was 100 milliamperes.

A series of discharge-chamber studies have been performed on both the SERT II and the cusp-field geometries. The first concern was whether a discharge could be ignited and operated at a reasonable argon flow rate. Although propellant utilization is not a primary concern as it is with thrusters, it is desirable to limit the gas flow rate to reduce pumping requirements. Nearly the same discharge-chamber performance has been obtained with the cusp-field geometry as with the SERT II geometry. Figures 10 and 11 show plots of discharge-chamber voltage as a function of anode current for five gas-flow rates. Tests indicated that the discharge chamber operated best (figs. 10 and 11) when the argon flow was split between the cathode region and the outer chamber. The cathode gave the best performance when it was positioned such that its end was even with of the cathode pole piece. The cusp-field source performed best with lower magnetic field on the grid end of the discharge chamber than at the cathode end.

ION-BEAM APPLICATIONS

Two types of processes were studied: sputter deposition and ion-beam sputter etching and machining. What follows is a series of experimental descriptions to illustrate some of the potential applications of this technology.

Table II shows a list of the materials that have been sputter deposited to date. Several different categories of materials are included - metals, semiconductors, insulators, and polymers. The sputter deposition rates were measured with a quartz crystal microbalance. The source beam current and energy at each measured rate are included in table II.

Table III shows a limited list of materials for which sputter etching rates were obtained. The etching rates were determined by placing a sample of material in the ion beam and then measuring the change in thickness after a known etching time.

The differences in source operating conditions in tables II and III are due to differences in the melting points, heat capacities, and thermal conductivities of the target materials. For example, Teflon must be sputtered at a low beam current to minimize the thermal decomposition of the polymer. Carbon, on the other hand, can be subjected to high beam currents and energy without damage. In fact, the low sputtering yield of carbon requires a more energic beam to achieve reasonable sputter deposition rates.

For metals and polymers, adherent deposition coatings were achieved with no substrate heating. Silicon dioxide and aluminum oxide required substrate heating to approximately 400° C to achieve adherent deposition coatings.

Generally, it is very useful to thoroughly clean substrates in the ion beam before initiating deposition. A unique advantage of ion-beam sputtering is its ability to go smoothly and quickly from substrate etching to deposition. This procedure, together with the high velocity of the sputtered atoms, results in very good adherence.

Figure 12 shows the variation of sputter deposition rates of aluminum and molybdenum as a function of ion-beam current. Measurements were made with a quartz-crystal microbalance at a point just outside the beam envelope. The deposition rate increases linearly for molybdenum and is a monotonically increasing function for aluminum. Molybdenum was also deposited onto a 46- by 46-centimeter piece of glass. The film thickness was subsequently measured and is plotted in figure 13. The results show that the deposition is skewed in the forward direction.

At beam currents above 150 milliamperes with V_I greater than or equal to 1000 volts, it was noted that thin metal targets began to glow. For lower melting point metals, such as aluminum, target cooling or a reduction in sputtering current would be required. A preliminary experiment was performed to evaluate the target cooling requirements. A 0.64-centimeter-thick aluminum target was mechanically clipped to a water-cooled copper target support. Figure 14 shows the variation in temperature as measured by a thermocouple embedded in the aluminum target with and without water-cooling. The waterflow rate was 16 milliliters per second. Figure 15 shows the target temperature as a function of beam power with watercooling. Figures 14 and 15 show target temperatures that can be achieved with a relatively simple water cooling system. Lower target temperatures would require more water flow or better heat transfer between target and cooling passages.

Sputter Deposition

Silicon. - Thin film silicon deposits are currently of great interest for ground-based solar-cell applications. If high-quality crystalline silicon films could be deposited over large areas at a reasonable cost, it would be a technological breakthrough of major significance. The basic problem is to deposit films of sufficiently large crystallite size such that electrons can be collected with reasonable efficiencies.

The first set of experiments that were performed used a test configuration (fig. 16(a)) where the silicon was located such that its surface was parallel to the surface of the target. The substrate heater (fig. 17) was used to raise the substrate temperature to about 1000° C. The substrate was heated to increase the surface mobility of the deposited silicon atoms and thereby increase the size of the silicon crystallites. The deposition procedure consisted of first cleaning the substrate by immersing it in the ion beam and then rotating it into position for deposition. The substrate heater was turned

on during this entire time. The resulting films were analyzed with an X-ray Bragg diffractometer; the measured grain sizes and crystal orientations are shown in table IV.

It was interesting that all the silicon deposits were of (110) orientation, particularly on the single-crystal silicon substrate, which was a (111) orientation. No epitaxial growth occurred. The orientations of the deposited films appeared to be independent of the substrate orientation.

An alternative technique for depositing silicon was also tried. The target was oriented at an oblique angle with respect to the beam and the substrate downstream of the target (fig. 16(b)). Because of oblique sputtering angles, the silicon atoms deposited onto the substrate were more energetic; it was thought that this greater mobility would lend itself to larger crystallites.

With oblique angle deposition, the substrate can be located in a position where it is etched by the beam when the target is rotated out of position. This allows a smooth and continuous operational transition from etching to deposition, which should eliminate any surface contamination of the substrate silicon interface. The target was at a 20° angle to the ion source axis.

Two samples were deposited using this technique: one with the substrate oriented such that the sputtered silicon arrived normally and the second with the substrate oriented such that the sputtered silicon arrived obliquely. Both deposits were on sapphire substrates. The results are tabulated in the second half of table IV. As shown, the crystallite sizes are smaller for the oblique deposits. Apparently, the greater energy of the oblique deposits did not translate into greater surface mobility.

Capacitor fabrication. - Another ion-beam sputtering application is the deposition of Teflon films. Capacitors have been fabricated by sandwiching a Teflon film between two aluminum films. Advances in integrated circuit technology have developed a need for small, high-energy-density capacitors. Thin-film capacitors (ref. 22) have the potential for filling this need, particularly if the technology can be developed for multiple layer capacitors.

Initially, capacitor fabrication was tried with silicon dioxide and aluminum oxide as the insulating layers, but, shortly thereafter Teflon insulating layers were chosen for study. The change in material resulted from the greater ease with which the Teflon insulating layers could be deposited. Achieving good adherence of silicon dioxide and aluminum oxide requires that the substrate temperature be about 400° C. The Teflon can be deposited with the substrates at room temperature. In addition, Teflon layers can be sputtered at much faster rates.

Considerable care is required to successfully fabricate thin-film capacitors, because the dimensions of surface contaminants and surface features must be kept small with respect to the film thicknesses (2000 Å). The substrate must be thoroughly cleaned. Our procedure was to scrub them in soapy water, rinse, ultrasonically clean in ethanol and blow them dry with Freon gas. The substrates were also blown with Freon gas to

remove dust each time before reinserting them into the vacuum system. Sapphire was chosen as the substrate material because its hardness makes it relatively scratch free. It is expected that the results can be duplicated on glass, but great care in substrate preparation and handling will be required.

The fixture used for capacitor fabrication is shown in figure 18. It allows the substrate and mask to be held separately. The substrate is held down with a bolt, and the masks slide in the channels shown. There is 1-millimeter clearance between the mask and the substrate. The space eliminates damaging the substrate or deposits during mask changes and also results in tapered film edges. Tapered film edges are preferred because its much easier to layer them without getting shorts between conducting layers at the film edges.

Figure 19 is a sketch of a capacitor composed of two 0.6-centimeter-wide, 1.25-centimeter-long aluminum films, with a 1.05- by 1.05-centimeter Teflon film between. The active area of the capacitor is 0.36 square centimeter. The aluminum films are 2000 Å thick. The sputter deposited Teflon was compared with the target material. Attenuated total reflectance showed that the infrared spectrums were identical. Electron spectroscopic chemical analysis (ESCA) showed that the ratio of fluorine atoms to carbon atoms is 2.3 for films deposited with a net accelerating voltage of 1000 volts and a beam current of 50 milliamperes. At 500 volts and 50 milliamperes the films had a fluorine to carbon ratio of 2.2. The characteristics of ion-beam sputtered Teflon were compared with those of radiofrequency (rf) sputtered materials, including Teflon (ref. 24), and were found to be nominally the same.

Table V is a comparison of bulk Teflon, rf sputtered Teflon (ref. 23), and ion-beam sputtered Teflon. The dielectric constants of the sputtered films fall in the same range of values, both types of sputtering yield constants larger than the bulk value. The value of the dielectric strength for ion-beam sputtered films is very conservative, yet it falls between the limits of the rf sputtered films and is more than six times the bulk value. The resistivity and dissipation factor of the bulk Teflon are better than the values for the sputtered films. Either sputtering process will result in some free carbon which might cause lower resistivities and higher dissipation factors.

Figure 20 shows the dependence of capacitance as a function of thickness. The measured capacitance agrees reasonably well with the inverse thickness dependence of the simple capacitor equation

$$C = \frac{K\epsilon_0 A}{d}$$

where K is the dielectric constant, ϵ_0 is the permittivity of free space, A is the active area, and d is the thickness. The measured values of the dielectric constant and the dissipation factor are plotted as functions of thickness in figure 21. The films are

those whose capacitances were plotted in figure 20. The variations appear random and independent of thickness with one exception: the dielectric constant for thickest film is near the bulk value.

Lubrication applications. - Three of the materials that have been sputter deposited, Teflon, molybdenum disulfide, and carbon (or graphite), are of interest as lubricants. Sputter deposition of Teflon was discussed in the previous section. Deposition rates as high as 500 Å per minute have been demonstrated. Questions remain about the composition of the films and their frictional characteristics. Attempts at sputtering molybdenum disulfide have been unsuccessful. The deposits that have resulted from these attempts are very hard, which indicates that dissociation of the molybdenum from the sulfur has occurred. Deposits have been examined at various source operating conditions and with different substrate (target) orientations, but no improvement in films was achieved. Attempts at sputtering carbon were more successful. Carbon has one of the lowest sputtering yields, and this property makes it very difficult to sputter deposit carbon at useful rates. With a beam current of 150 milliamperes, a net accelerating voltage of 2000 volts, and the target oriented at 45° with respect to the beam, adherent coatings of carbon have been deposited at rates of 300 Å per minute.

Corrosion applications and dielectric coatings. - Ion-beam sputter deposition lends itself quite naturally to applying adherent coatings of insulating materials such as silicon dioxide and aluminum oxide. At source operating conditions of 2000 volts net accelerating potential and beam current of 190 milliamperes, sputter deposition rates of 950 Å per minute for silicon dioxide and 250 Å per minute for aluminum oxide have been achieved on metal substrates. Teflon deposition, discussed in an earlier section, has also been performed successfully on metal substrates.

These insulating materials have very useful dielectric characteristics. Measurements need to be made on the dielectric properties of these deposited film materials so that they can be compared with bulk values. The properties to be measured are dielectric constant, dielectric strength, and dissipation factor.

Preliminary experiments have been performed with the ion-beam sputtering of Parylene monomer (ref. 25). The objectives of future experiments will be to determine if the ion beam can simultaneously provide the heating required for polymerization and the momentum for mass transfer.

Material mixtures. - It is possible to create composite materials by simultaneously sputtering targets that composed more than one material (fig. 22). The sputter deposits that result will be atomically mixed combinations of the target materials. Any combination of solid materials is possible. Such combinations as aluminum-copper and Teflon-copper have been deposited. This technique can create a whole new class of materials, some of which may have interesting and useful properties. The relative ratio of constituents is determined by the area struck by the ion beam and the relative ratio of sputtering yields.

Other deposition applications. - Figure 23 is a picture of a stainless-steel grid that was deposited onto a spacecraft thermal control surface to prevent electrical charging of the insulating surface in space. In addition, the deposition of a 5-micrometer-thick copper deposit on a microwave cavity for electron spin resonance has been performed.

Sputter Etching and Machining

Ion-beam machining as used herein refers to a set of processes where the work piece is immersed directly in the ion beam. Some examples of this include ion-beam cleaning of silicon for the integrated circuits, ion milling of diffraction gratings, and polishing of laser mirrors.

Ion-beam cleaning and etching. - One of the first experiments performed was the ion-beam etching of silicon. Ion beam etching does not damage the surface by inducing strains, and it etches uniformly in contrast to chemical processes. Removing the surface silicon oxide layer in vacuum is desirable to insure a clean silicon surface for subsequent procedures.

Another experiment performed was the etching of stainless steel using a colloidal suspension of carbon as a sputter mask. First, the commercial suspension was sprayed onto the metal surface, after drying, letters were scratched through the carbon coating. After the surface was immersed in the ion beam, the metal exposed by the scratches was sputtered at a much faster rate than the carbon coating. The net result was that the letters were etched into the metal.

Ion-beam polishing. - Seven metal samples, aluminum, copper, brass, tantalum, iron, and galvanized and stainless steel, were first sandblasted to provide a uniform, well-defined roughness and then polished with an ion beam. The sandblasting conditions were as follows: 50-micrometer silicon carbide grit, 55.2-newton-per-square-centimeter pressure, and 350-milligram-per-minute feedrate with the nozzle perpendicular to the metal surface and positioned 2.5 centimeters away. The samples were then cut in half; one half was retained for documenting the initial surface roughness, and the other half for ion polishing. The seven samples were mounted with the ion beam tangential to the sample surfaces. The beam preferentially sputters the high points, polishing the surface. The samples were polished for 24 hours at a net accelerating voltage of 1000 volts and a beam current of 100 milliamperes. After polishing, the samples were examined using a scanning electron microscope (SEM). Photomicrographs of the before and after polishing conditions of brass and tantalum are shown in figure 24. Two results were immediately noted from the micrographs. First, not surprisingly, the softer materials were more readily polished; and second, the polished surfaces appeared channeled or grooved. The second result strongly suggests the need for rotating the samples during polishing.

Ion-beam drilling. - Figure 25 shows a carbon mask that was used for drilling irregularly shaped holes in stainless steel. The mask was placed over a piece of stainless steel and oriented with the ion beam perpendicular to its surface. Because stainless-steel sputters at a much faster rate than carbon, holes can be drilled in the stainless with very little change in the mask thickness. The experiment was operated for 75 hours at a net accelerating voltage of 1000 volts and a beam current of 100 milliamperes. The etching rate of the stainless steel was 2100 Å per minute.

Ion-beam sawing. - Ion-beam sawing was performed on one tab of an integrated circuit to verify the integrity of the gold plating without smearing the interface as would occur with mechanical means. The lead was partially masked by a thin sheet of carbon and then placed in the ion beam. The experimental arrangement is shown in figure 26. After 10 hours the beam successfully sliced off the lead, exposing its cross section. Figure 27 is an SEM photograph of the cross section that resulted from ion-beam sawing and a similar tab that was mechanically cut. Figure 28 is another SEM photograph of the gold-Kovar interface. Ion-beam sawing lends itself particularly well to very small or fragile samples that would present a considerable challenge to standard sample preparation techniques.

Surface Texturing

Under certain conditions, microscopic cone and needle structures can be created on target materials by an ion beam (refs. 26 and 27). A cone structure can be caused to form on silicon by simultaneously sputter depositing tantalum onto the silicon and etching it. What results is the field of microscopic cones shown in figure 29. Table VI shows some of the primary dimensions of the cone structure. The cones on the silicon surface make it appear black. The resulting cone structure is strongly dependent on the tantalum arrival rate. Figure 30 is an SEM photograph of a silicon surface that was etched with a lower tantalum arrival rate. The cone density was greatly reduced. When the silicon surface was first coated with tantalum, and then etched, the resulting structure is much different (fig. 31).

Similar cone structures have been created in aluminum, stainless steel, copper, and gold. These structures are shown in figure 32. The photomicrographs attest to considerable differences among the materials. Aluminum and stainless steel appear more like needles than cones. There was also considerable variation in cone heights. The optical appearance of a cone covered surface is very direction dependent. The reflectance is a minimum when viewed along the axis of the cone structures. Figure 33 shows the change in stainless-steel reflectance as a result of sputter etching. This type of surface treatment could be used to modify reflectance and emissivity, to increase surface area (possibly increasing absorption characteristics), to enhance thermionic emission, to

enhance thermal conductivity, and to promote adhesion by microscopic roughening a surface.

CONCLUDING REMARKS

Ion propulsion research and development yields a mature technology that is transferable to a wide range of nonpropulsive applications, including terrestrial and space manufacturing. In this work, a xenon ion source was used for an investigation into potential ion-beam applications. An argon source development program was initiated and will be the subject of future work.

An 8-centimeter-diameter ion-beam source has demonstrated its ability to sputter deposit several materials, such as aluminum oxide, silicon dioxide, carbon, and Teflon, that are difficult to sputter deposit by other techniques. Capacitors have been successfully fabricated by sputter deposition of Teflon. Present efforts are directed toward defining the thickness dependence of the capacitance and evaluating the dielectric field strength. Preliminary experiments on ion-beam polishing were successful, and further enhancement of the polishing process will probably require sample rotation. The creation of a microscopic cone structure is unique to sputtering and can best be obtained by the ion-beam process. This type of surface treatment may have numerous applications.

Lewis Research Center,
National Aeronautics and Space Administration,
Cleveland, Ohio, November 30, 1976,
506-22.

REFERENCES

1. Kaufman, Harold R.: An Ion Rocket with an Electron-Bombardment Ion Source. NASA TN D-585, 1961.

2. Gold, Harold; et al.: Description and Operation of Spacecraft in SERT I Ion Thruster Flight Test. NASA TM X-52050, 1964.

3. Kerslake, W. R.; Goldman, R. G.; and Nieberding, W. C.: SERT II - Mission Thruster Performance and In-Flight Thrust Measurements. J. Spacecr. Rockets, vol. 8, no. 3, March 1971, pp. 213-224.

4. Goldman, R. G.; Gurski, G. S.; and Hawersaat, W. H.: Description of SERT II Spacecraft and Mission. AIAA Paper 70-1124, Aug. 1970.

5. Kerslake, W. R.; and Finke, R. C.: SERT II Hollow Cathode Multiple Restarts in Space - Stationkeeping and Primary Electric Propulsion. AIAA Paper 73-1136, Oct. 1973.

6. Sovey, J. S.; and King, H. J.: Status of 30 cm Mercury Ion Thruster Development. AIAA Paper 74-1117, Oct. 1974.

7. Banks, B. A.: 8-cm Mercury Ion Thruster System Technology. AIAA Paper 74-1116, Oct. 1974.

8. Collett, C. R.: A 7700 Hour Endurance Test of a 30-cm Kaufman Thruster. AIAA Paper 75-366, Mar. 1975.

9. Nakanishi, S.: A 15 000-Hour Cyclic Endurance Test of an 8-Centimeter-Diameter Electron Bombardment Mercury Ion Thruster. AIAA Paper 76-1022, Nov. 1976.

10. Wintucky, E. G.: A 20,000-Hour Endurance Test of a Structurally and Thermally Integrated 5-cm-Diameter Ion Thruster Main Cathode. AIAA Paper 75-368, Mar. 1975.

11. Laznovsky, W.: Advances in Low-Energy Ion-Beam Technology. Res./Dev., vol. 26, no. 8, Aug. 1975, pp. 47-55.

12. Reader, Paul D.; and Kaufman, Harold R.: Optimization of an Electron-Bombardment Ion Source for Ion Machining Applications. J. Vac. Sci. Technol., vol. 12, no. 6, Nov.-Dec. 1975, pp. 1344-1347.

13. Garvin, Hugh L.: High Resolution Fabrication by Ion-Beam Sputtering. Solid State Technol., vol. 16, no. 11, Nov. 1973, pp. 31-36.

14. Spencer, E. G.; Schmidt, P. H.; and Fisher, R. F.: Microstructure Arrays Produced by Ion Milling. Appl. Phys. Lett., vol. 17, no. 8, Oct. 1970, pp. 328-334.

15. Farmsworth, H. E.; et al.: Application of the Ion Bombardment Cleaning Method to Titanium, Germanium, Silicon, and Nickel as Determined by Low-Energy Electron Diffraction. J. Appl. Phys., vol. 29, no. 8, Aug. 1958, pp. 1150-1161.

16. Hoffman, R. A.; Lange, W. J.; and Choyke, W. J.: Ion Polishing of Copper: Some Observations. Appl. Opt., vol. 14, no. 8, Aug. 1975, pp. 1803-1807.

17. Yasuda, Hiroshi: Figuration of Wedged-Shaped and Parabolic Surfaces by Ion Etching. Jpn. J. Appl. Phys., vol. 12, no. 8, Aug. 1973, pp. 1139-1142.

18. Beattie, J. R.; and Wilbur, P. J.: 15 cm Cusped Magnetic Field Mercury Ion Thruster Research. AIAA Paper 75-429, Mar. 1975.

19. Kaufman, Harold R.: Experimental Investigations of Argon and Xenon Ion Sources. (Colorado State Univ.; Grant NsG-3011) NASA CR-134845, 1975.

20. Weigand, Albert J.; and Nakanishi, Shigeo: A Survey of Kaufman Thruster Cathodes. NASA TM X-67918, 1971.

21. Bechtel, Robert T.: Discharge Chamber Optimization of the SERT II Thruster. AIAA Paper 67-668, Sept. 1967.

22. Maissel, Leon; and Glang, Reinhard: Handbook of Thin Film Technology. McGraw-Hill Book Co., Inc., 1970.

23. Miller, R. I.; and Ruff, R. C.: Effects of Sputtering Parameters on Teflon Thin Film Capacitors. NASA TM X-53937, 1970.

24. Coburn, J. W.; Eckstein, E. W.; and Kay, Eric: A Mass Spectrometric Study of Neutral-Sputtered Species in an rf Glow Discharge Sputtering System. J. Vac. Sci. Technol., vol. 12, no. 1, Jan.-Feb. 1975, pp. 151-154.

25. Cariou, F. E.; Valley, D. J.; and Loeb, W. E.: Poly-Para-Xylylene in Thin Film Applications. IEEE Trans. Parts, Mater. Packag., vol. PMP-1, no. 1, June 1965, pp. 54-62.

26. Wehner, G. K.; and Hajicek, D. J.: Cone Formation on Metal Targets During Sputtering. J. Appl. Phys., vol. 42, no. 3, Mar. 1971, pp. 1145-1149.

27. Berg, R. S.; and Kominiak, G. J.: Surface Texturing by Sputter Etching. J. Voc. Sci. Technol., vol. 13, no. 1, Jan.-Feb. 1976, pp. 403-405.

TABLE I. - XENON SOURCE OPERATING RANGE

Net accelerating potential, V_I, V	500 - 2000
Beam current, J_B, mA	10 - 200
Xenon flow rate, $\dot{m}_c$, std. cm^3/min	2.0
Discharge voltage, ΔV_I, V	45
Discharge current, J_E, A	0.35 - 1.5
Discharge losses, ϵ, eV/ion	330
Propellant utilization, η_u, percent	60
Accelerator voltage, V_A, V	-200 - -500
Accelerator current, J_A, mA	0.63 - 1.5
Neutralizer coupling potential, V_G, V	15
Cathode heating power, P_{CH}, W:	
Starting	40
Operating	15
Cathode keeper voltage, V_{CK}, V	14
Cathode keeper current, J_{CK}, A	0.2
Neutralizer heater power, P_{NH}, W:	
Starting	50
Operating	25
Neutralizer keeper voltage, V_{NK}, V	15
Neutralizer keeper current, J_{NK}, A	0.4

TABLE II. - SPUTTER DEPOSITION RATES

[Determined with xenon sputtering source.]

Material	Source beam		Deposition rate, Å/min
	Current, mA	Energy, kV	
Aluminum	150	1	1460
Copper	↓	1	1930
Carbon		2	300
Gold		1	1130
Silicon	185	2	1170
Molybdenum	165	1	585
Teflon	50	1	250
Aluminum oxide	190	2	250
Quartz	190	2	950

TABLE III. - SPUTTER ETCHING RATES

[Determined with xenon etching source.]

Material	Source beam		Sputter etch rate, cm/min
	Current, mA	Energy, kV	
Gold	150	1	10.0×10^{-5}
Silicon	185	2	1.5
Stainless steel	150	2	8.5
Sapphire	190	2	.99
Tantalum	150	2	11.2

TABLE IV. - SILICON CRYSTALLITE SIZE

[Crystallite orientation, (110).]

Deposition angle	Substrate	Crystallite	
		Size, Å	Thickness, μm
Normal	Al_2O_3	1000	2
	SiO_2	880	10
	Si	450	12
Oblique	Al_2O_3, normal	200	2
	Al_2O_3, oblique	240	2

TABLE V. - COMPARISON OF BULK, SPUTTERED,

AND ION-BEAM SPUTTERED TEFLON

Teflon form	Dissipation factor	Resistivity, ρ, Ω-cm	Dielectric strength, ΔV_{BD}, kV/cm	Dielectric constant, K
Bulk	0.0002	1.9×10^{19}	157	2.1
rf sputtered films	0.005 - 0.05	1×10^{13} - 1×10^{15}	200 - 5000	1.4 - 7.4
Ion beam sputtered films	0.002 - 0.008	1×10^{12}	1000	1.4 - 6.8

TABLE VI. - DIMENSIONS OF ION BEAM ETCHED CONES IN SILICON

Cone height, cm	8.3×10^{-4}
Cone diameter, cm	1.7×10^{-4}
Apex angle, deg	45 - 50
Cone density, cones/cm^2	3.2×10^{3}

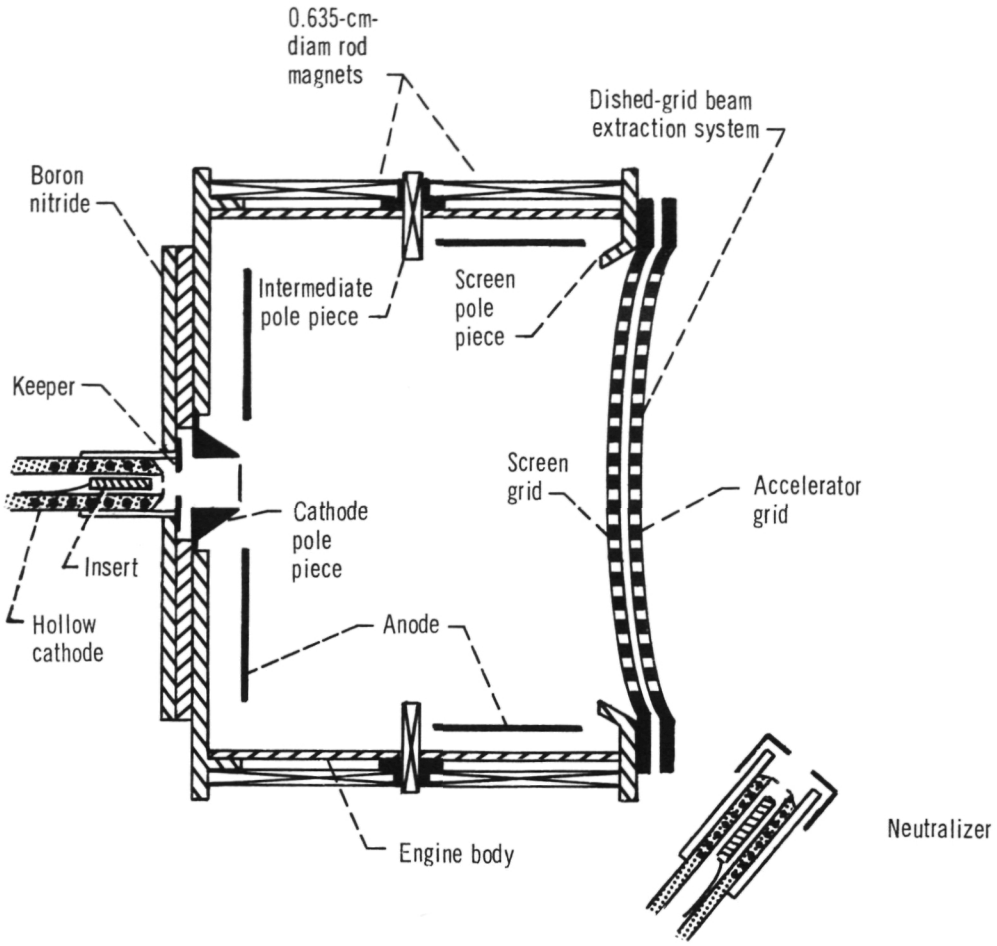

Figure 1. - Cross section of 8-centimeter-diameter source with a cusp magnetic field discharge chamber and a dished-grid beam extraction system.

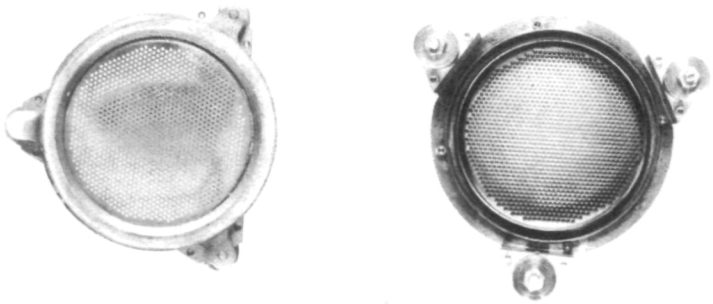

(a) From accelerator grid side.

(b) From screen grid side.

Figure 2. - Photographs of 8 centimeter optics.

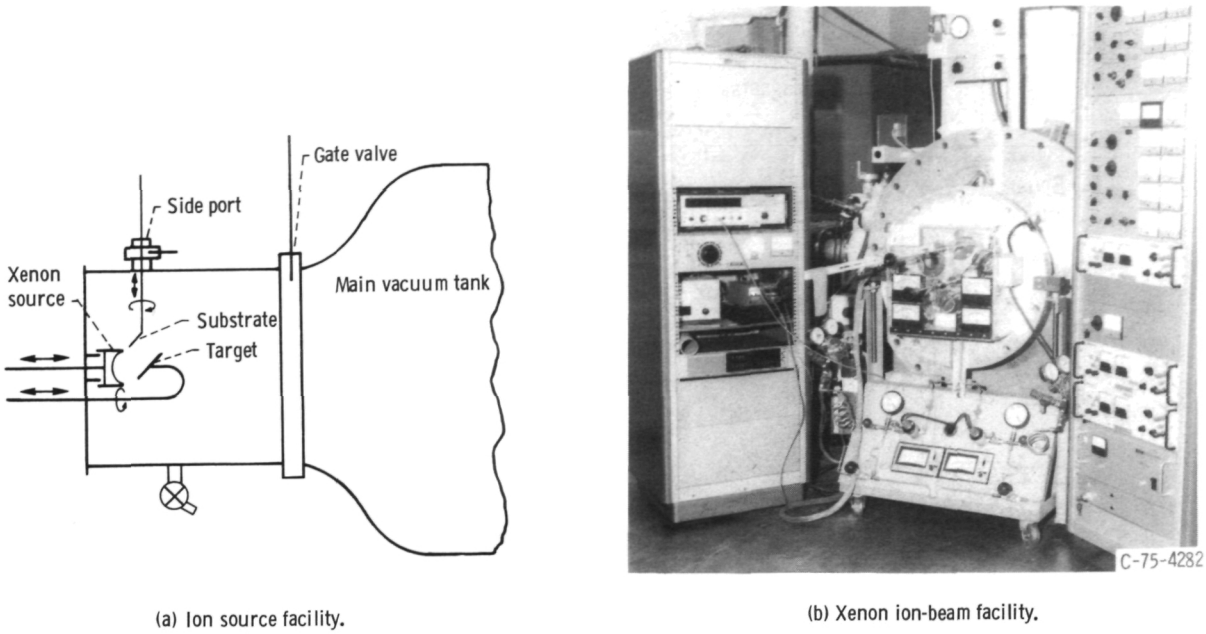

(a) Ion source facility.

(b) Xenon ion-beam facility.

Figure 3. - Operational arrangement.

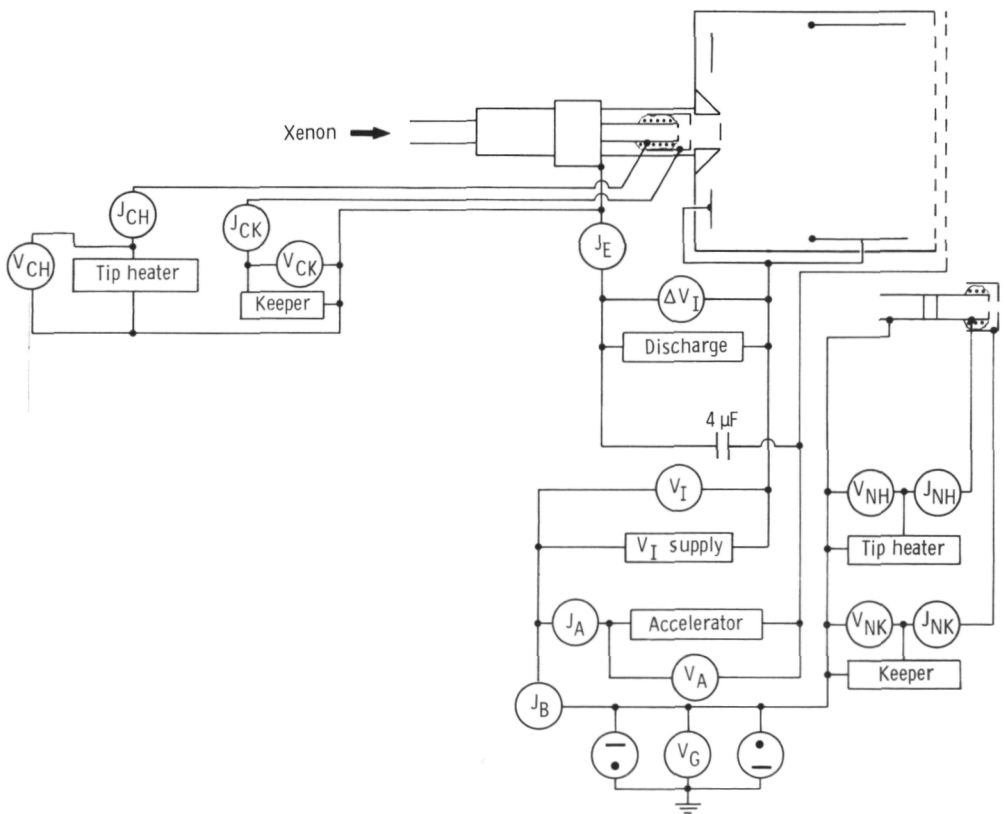

Figure 4. - Electrical circuit used for xenon source.

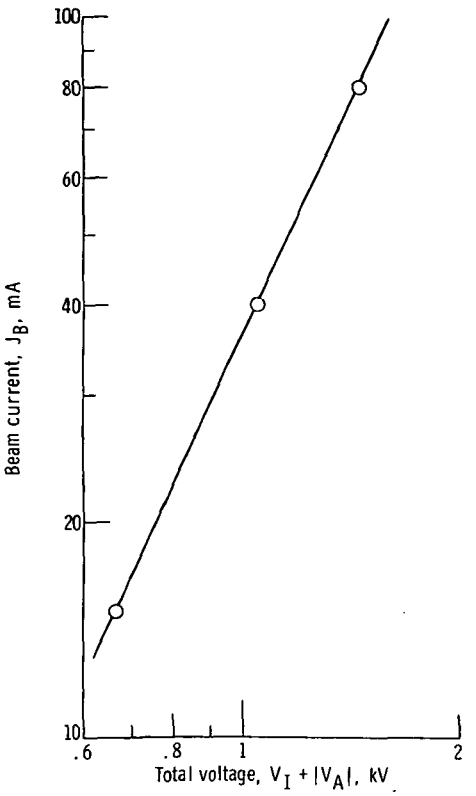

Figure 5. - Ion-beam current dependence on total voltage for an 8-centimeter-diameter xenon source.

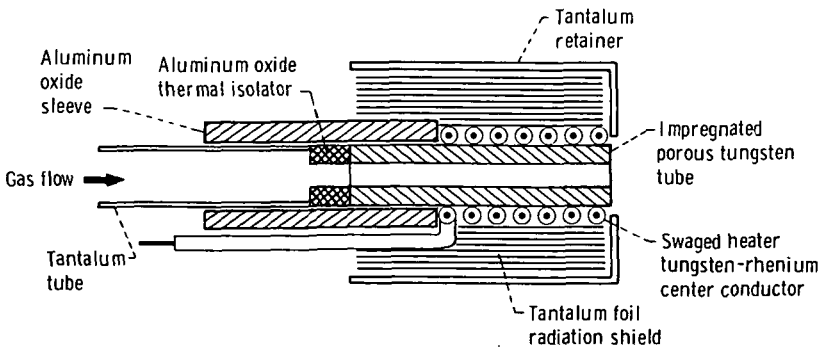

Figure 6. - Impregnated porous tungsten emitter in cross section. Emissive impregnate mole ratios, 4 barium oxide, 1 calcium oxide, 1 aluminum oxide.

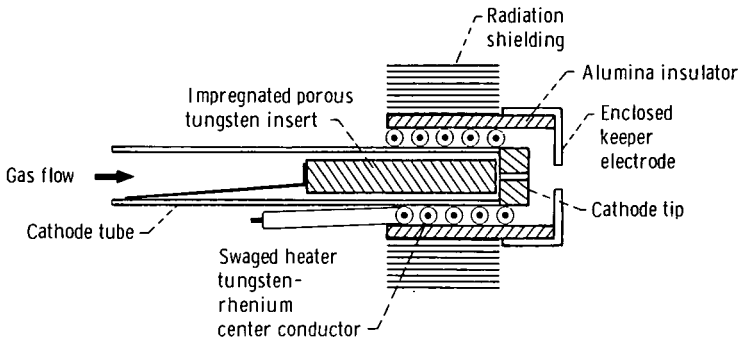

Figure 7. - Cross section of hollow cathode use as both main cathode and neutralizer on xenon source.

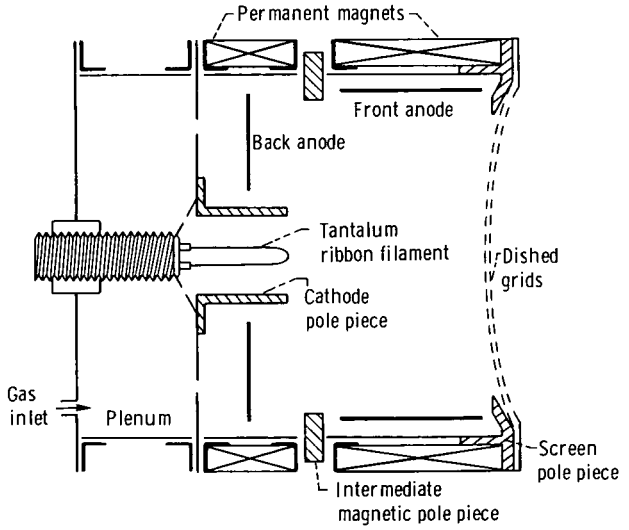

Figure 8. - Cross section of cusp field geometry source.

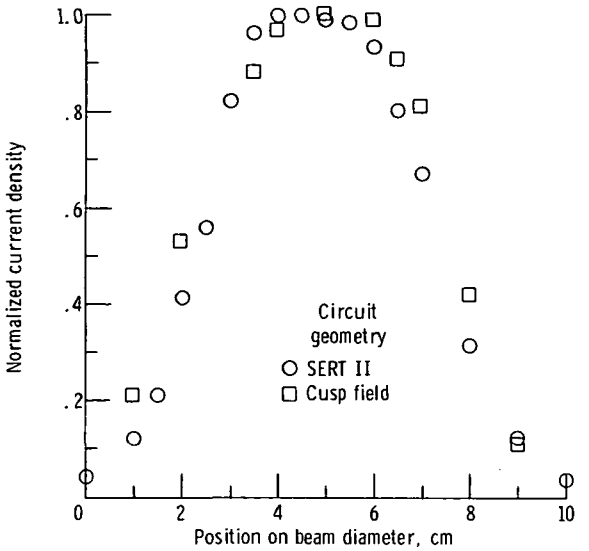

Figure 9. - Xenon source beam profile. Normalized current density with respect to position along beam diameter. All data taken with beam probe 5 centimeters downstream of the accelerator grid; net accelerating potential, 1000 volts; accelerator voltage, 250 volts; beam current, 100 milliamperes.

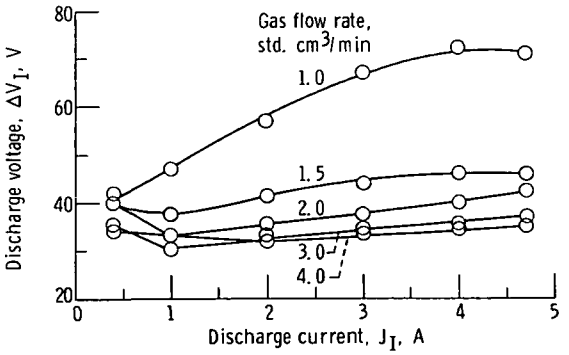

Figure 10. - Discharge chamber characteristics for SERT II geometry with argon gas.

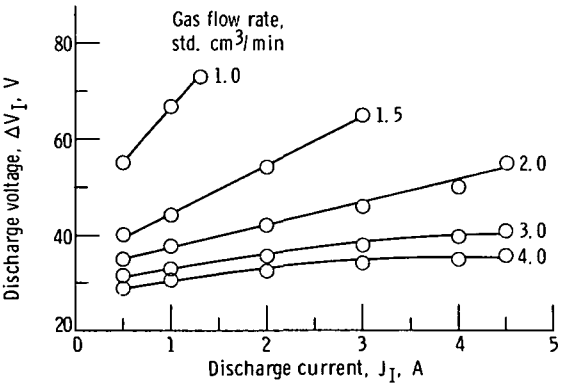

Figure 11. - Discharge chamber characteristics for cusp-field geometry with argon gas.

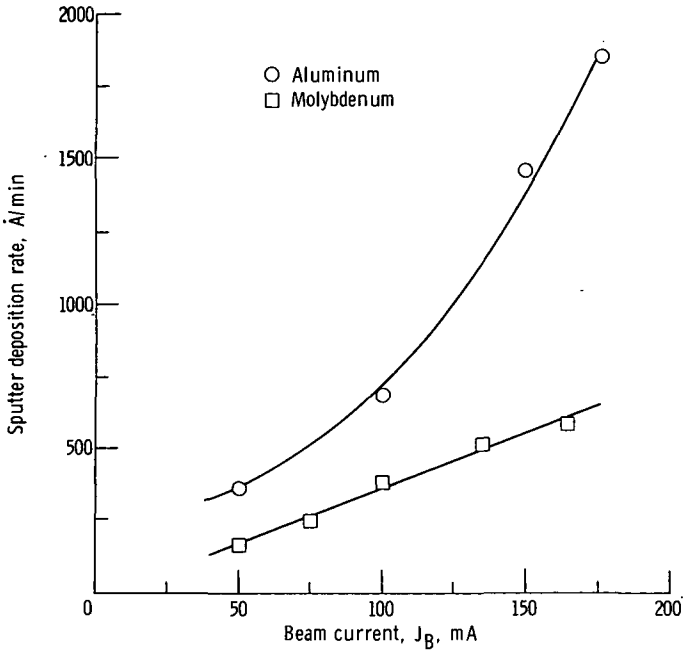

Figure 12. - Sputter deposition rates of aluminum and molybdenum as function of ion-beam current. Measurements were made using quartz crystal microbalance.

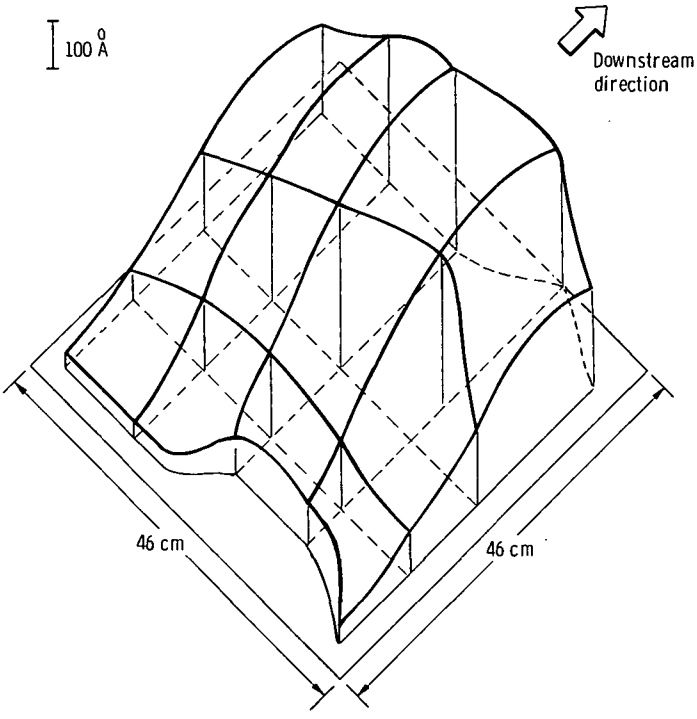

Figure 13. - Film thickness distribution using 8-centimeter-diameter xenon source. The molybdenum flux was normal to the substrate surface.

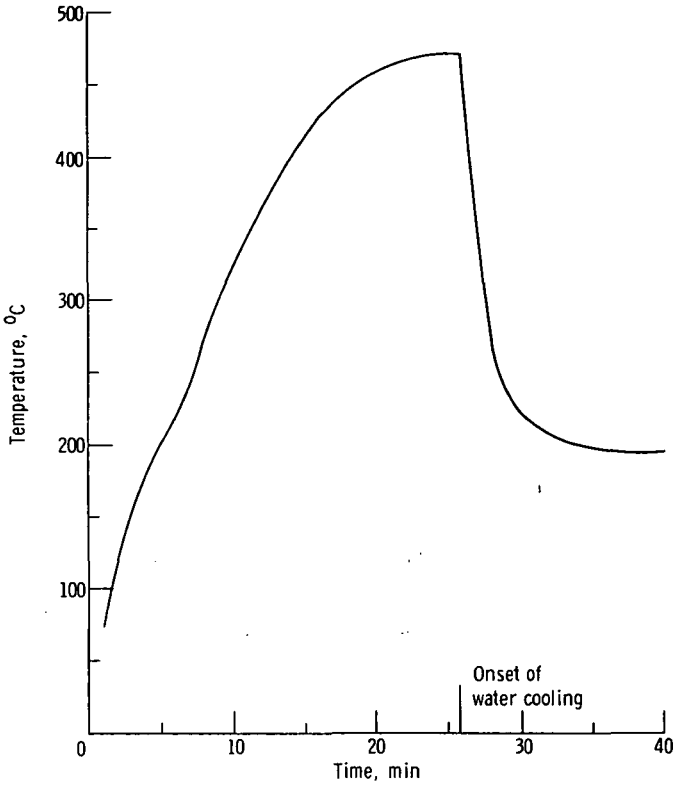

Figure 14. - Curve shows beam heating of 0.64-centimeter-thick aluminum target. Discharge voltage, 1000 volts; beam current, 100 milliamperes; water cooling was turned on at 26 minutes; target cooled to 195° C.

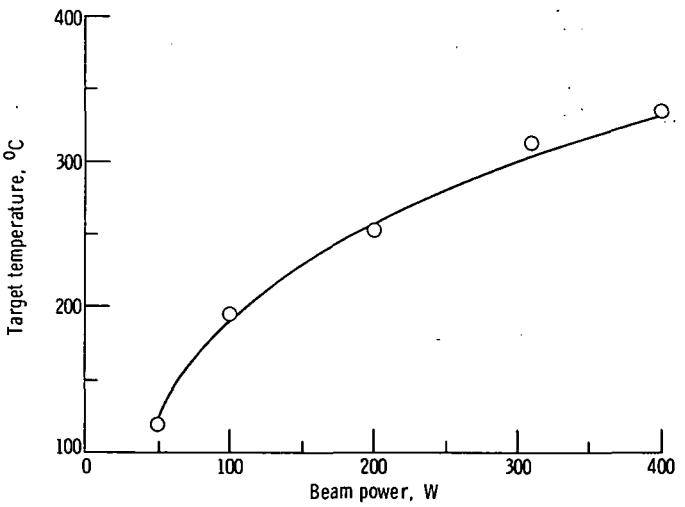

Figure 15. - Target temperature versus beam power with 16-milliliter-per-second water cooling. (Same target as used for fig. 14 data.)

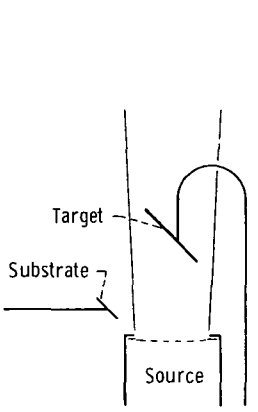

(a) Substrate opposite target - surfaces parallel.

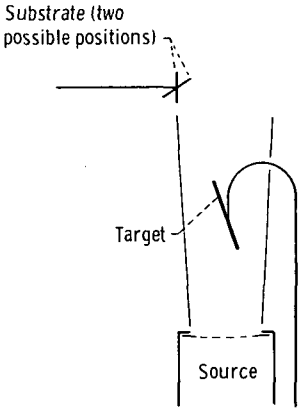

(b) Substrate downstream of target - substrate surface either oblique or perpendicular to target efflux.

Figure 16. - Two test configurations used for deposition of silicon films.

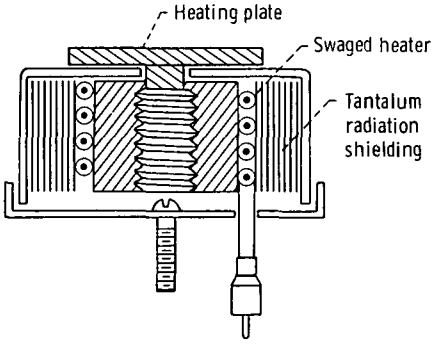

Figure 17. - Cross section of substrate heater assembly.

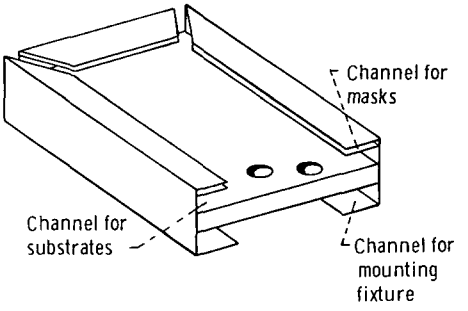

Figure 18. - Fixture used for capacitor fabrication.

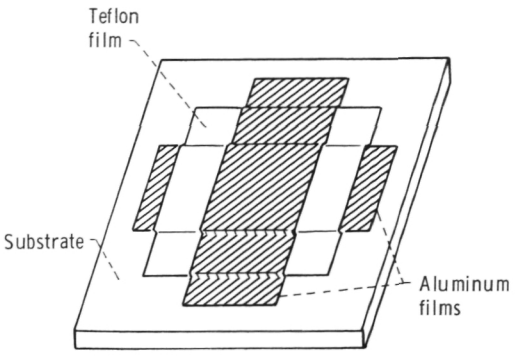

Figure 19. - Sketch of thin-film Teflon capacitor.

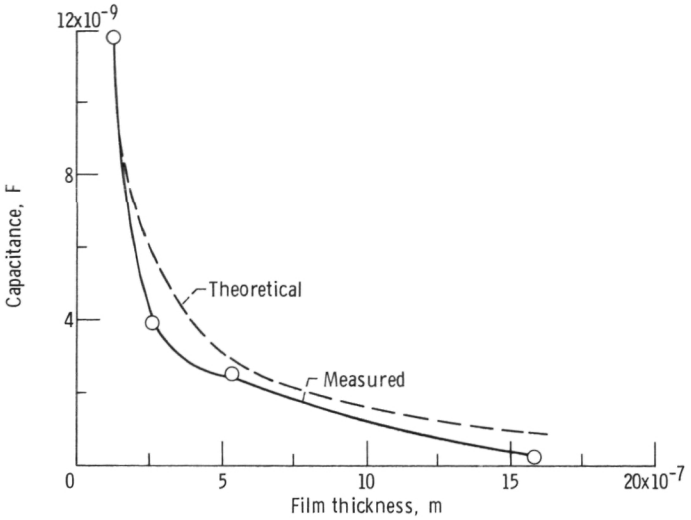

Figure 20. - Measured capacitance as function of thickness. The dashed line is an inverse thickness dependence.

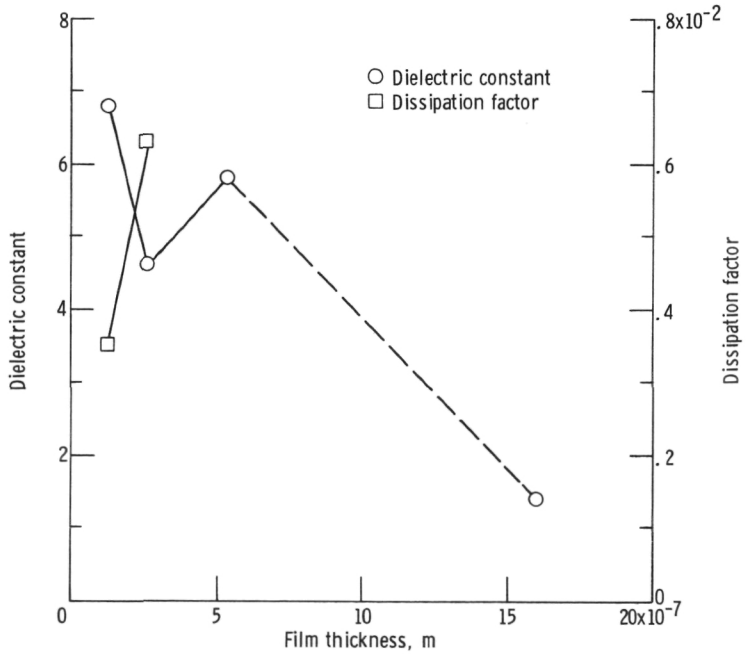

Figure 21. - Dielectric constant and dissipation factor as functions of thickness.

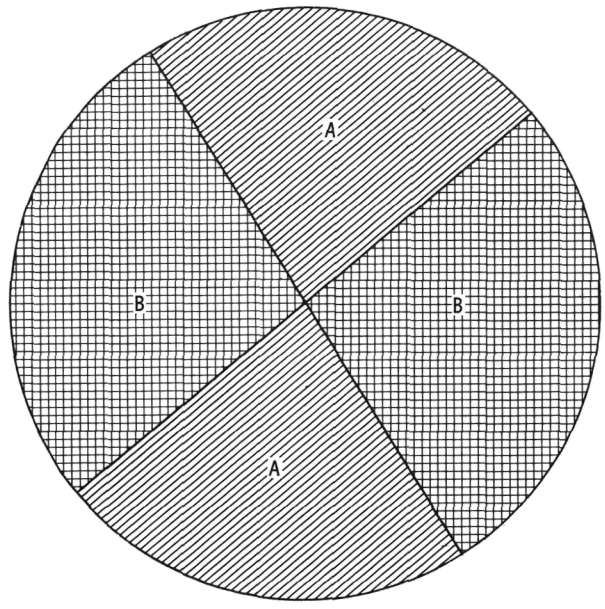

Figure 22. - Beachball multiple material targets.

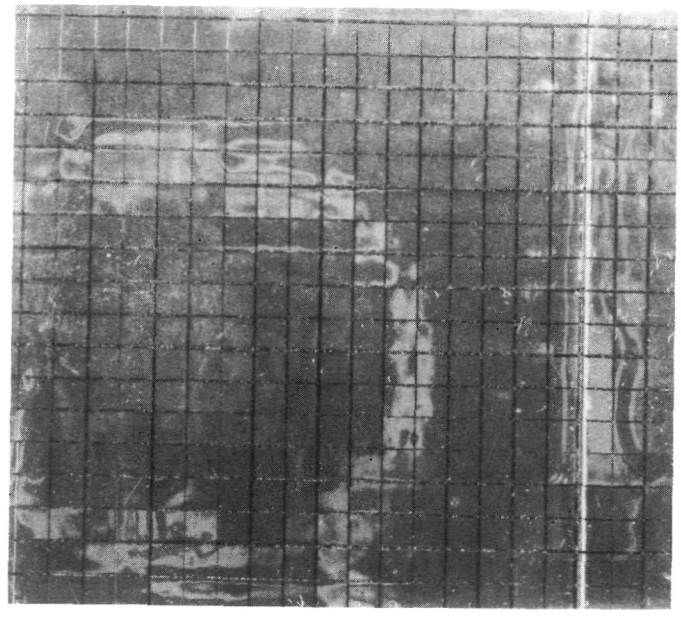

Figure 23. - Stainless-steel grid that was deposited on spacecraft thermal surface to prevent electrical charging.

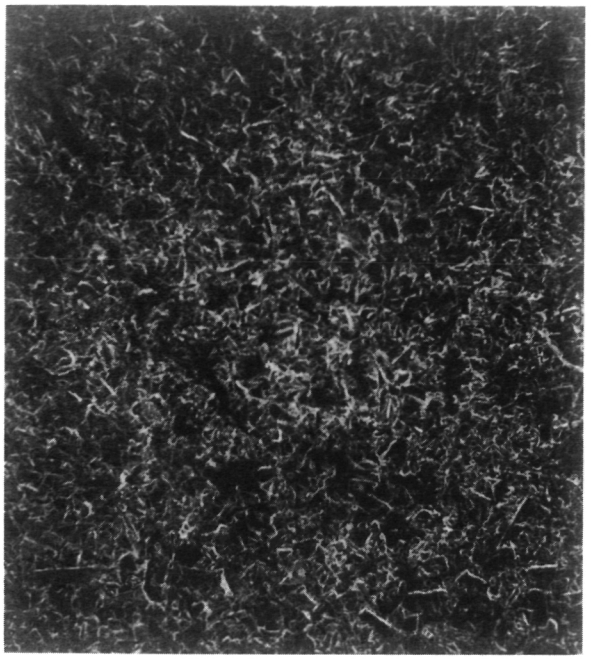

Grit blasted brass

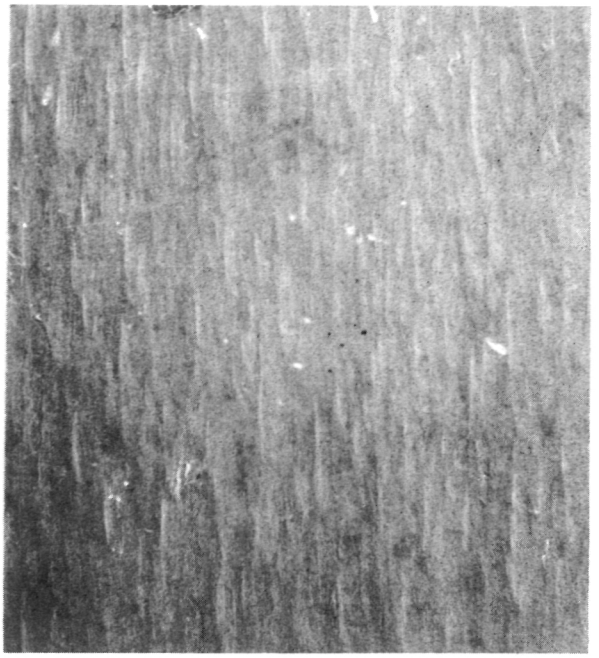

Ion polished tantalum

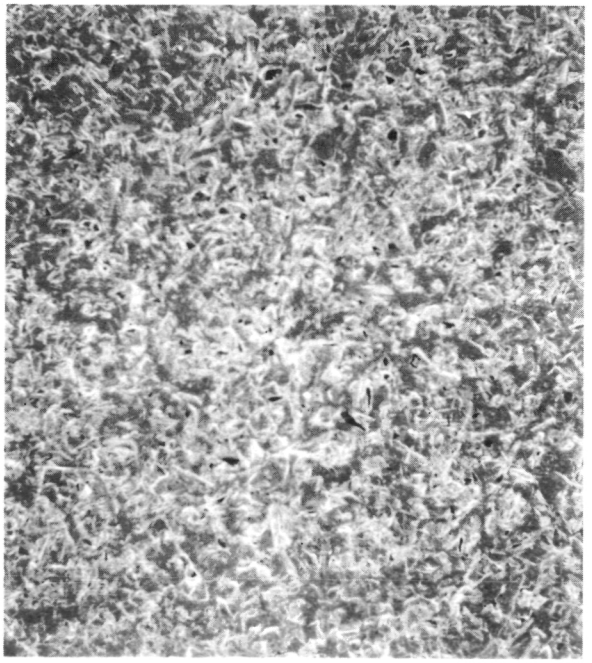

Grit blasted tantalum

Ion polished brass

Figure 24. - Scanning electron microscope photomicrographs of brass and tantalum before and after ion beam polishing.

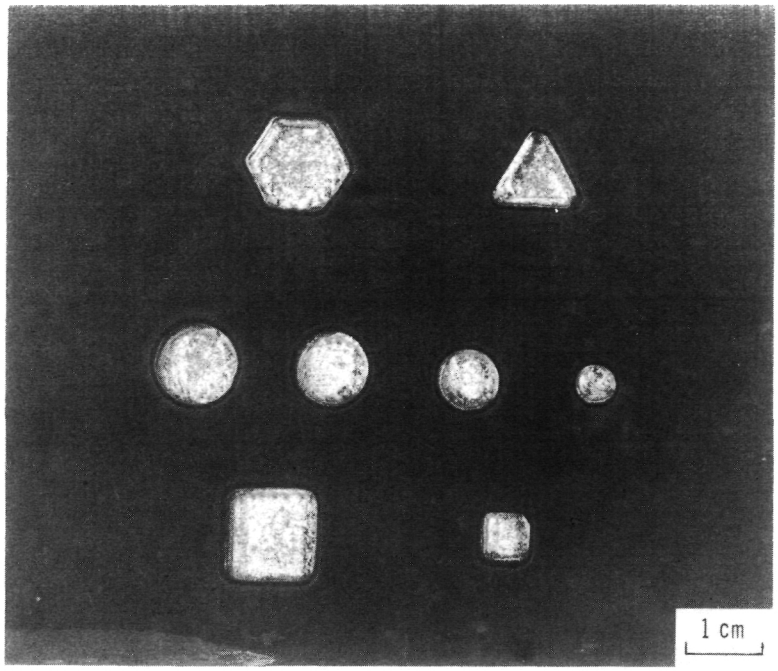

Figure 25. - Carbon mask covering a stainless-steel sheet that has been exposed to ion beam for 75 hours. Net accelerating voltage, 1000 volts; beam current, 100 milliamperes. Holes are 0.9 millimeter deep in stainless steel sheet. Carbon mask, 0.5 millimeter thick.

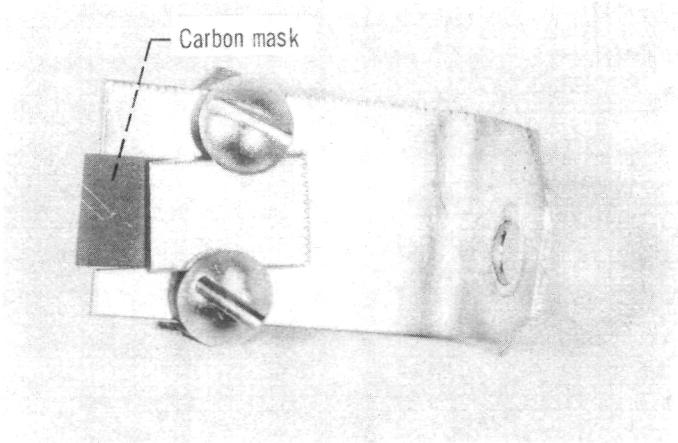

Figure 26. - The experimental fixture used for ion-beam sawing. Carbon mask used to clamp electrical lead.

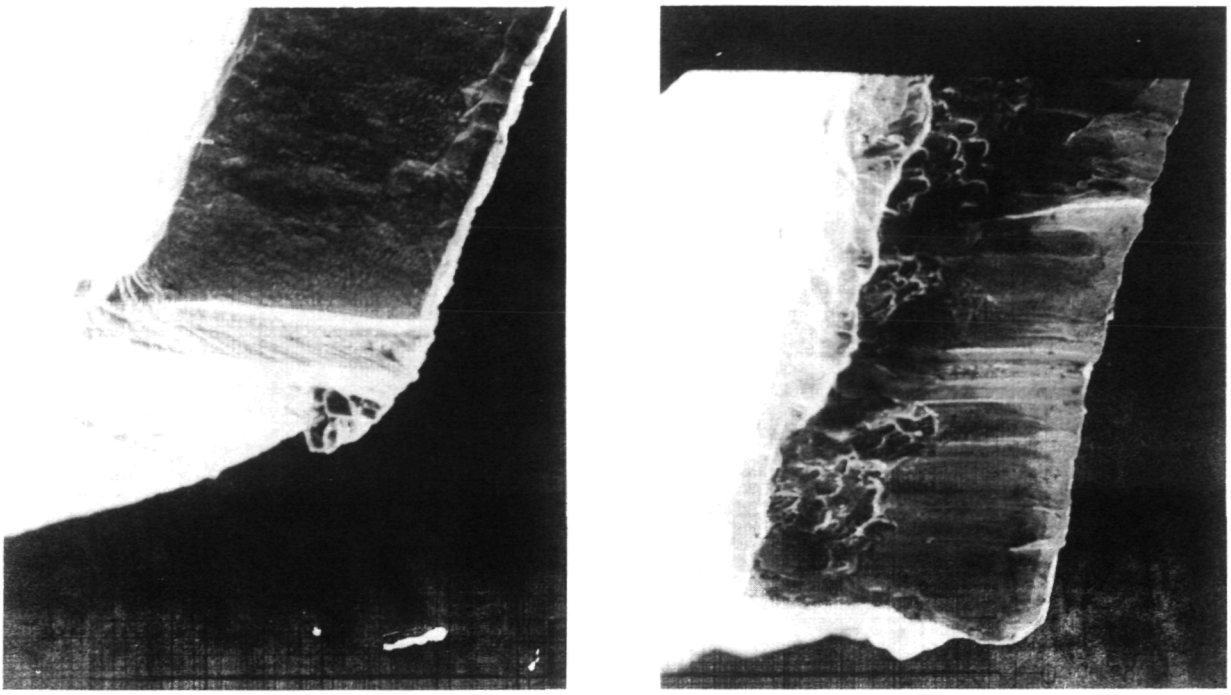

Ion-beam sawed

Mechanically sheared

Figure 27. - Scanning electron microscope photograph of electrical lead cross sections that resulted from ion-beam sawing and mechanically shearing. ×300.

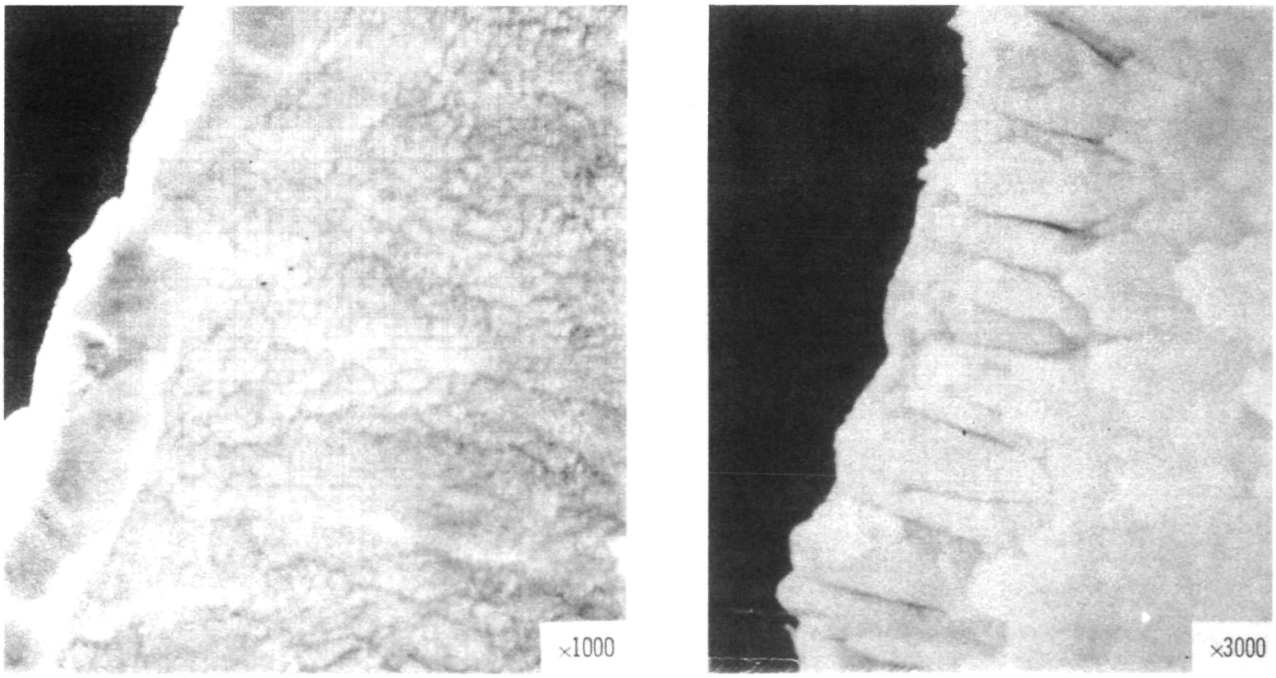

Figure 28. - Scanning electron microscope photomicrographs of gold/Kovar interface and of edge view of gold coating.

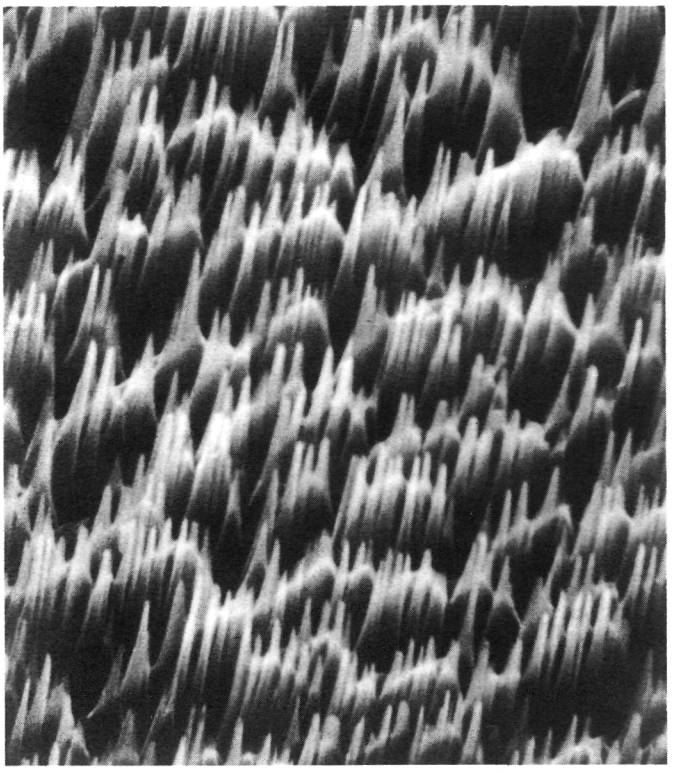

Figure 29. - Scanning electron microscope photomicrograph of cones etched in silicon by simultaneously etching in beam while sputtering tantalum onto silicon surface. ×6000.

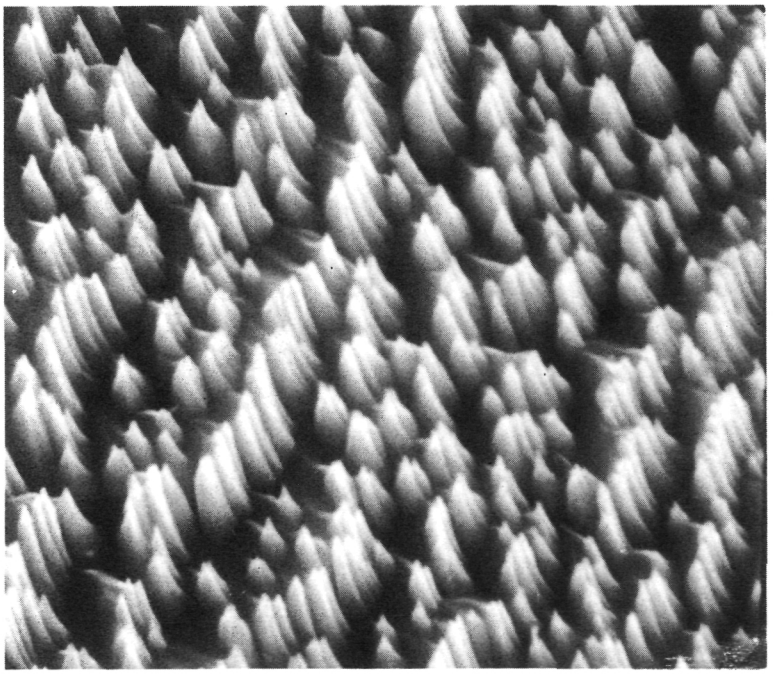

Figure 30. - Scanning electron microscope photograph of region of low cone density on ion-beam etched silicon. ×3000.

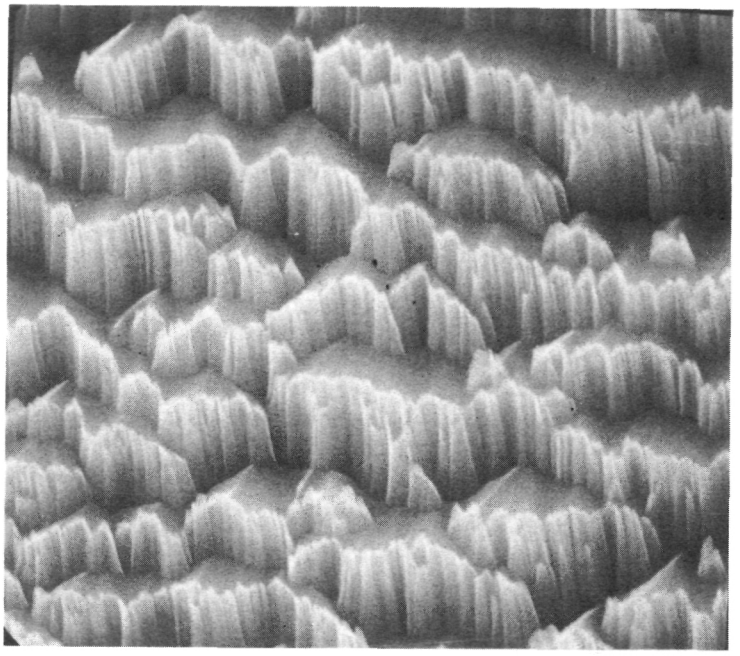

Figure 31. - Scanning electron microscope photograph of ion-beam etched silicon surface after first depositing tantalum and then etching. ×3000.

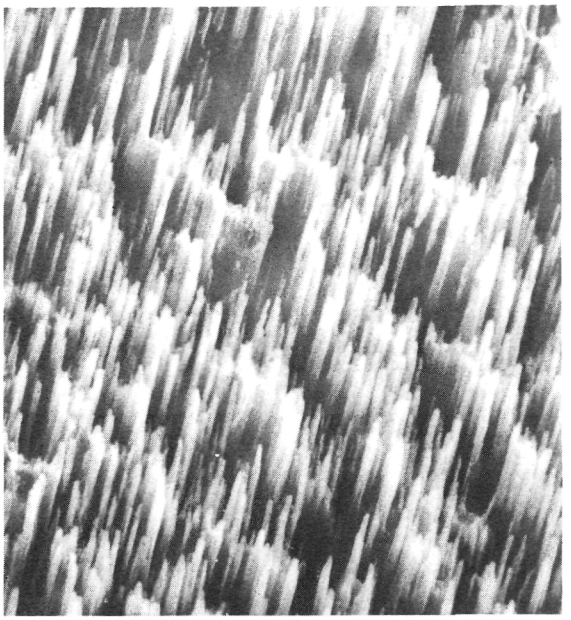

(a) Cones etched in aluminum.

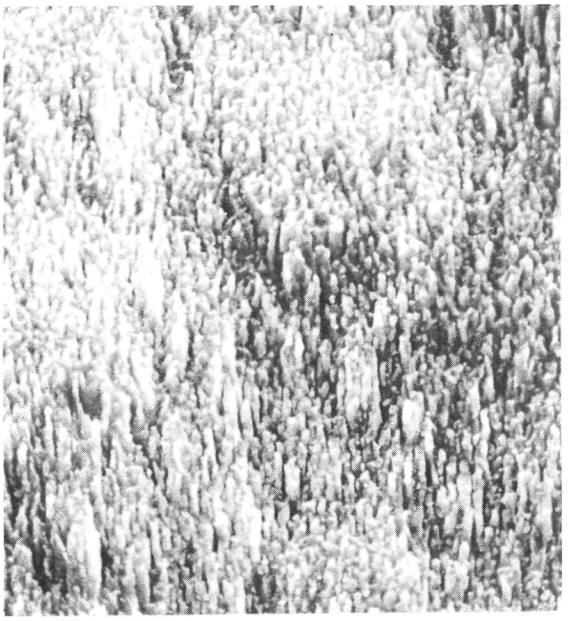

(b) Cones etched in stainless steel.

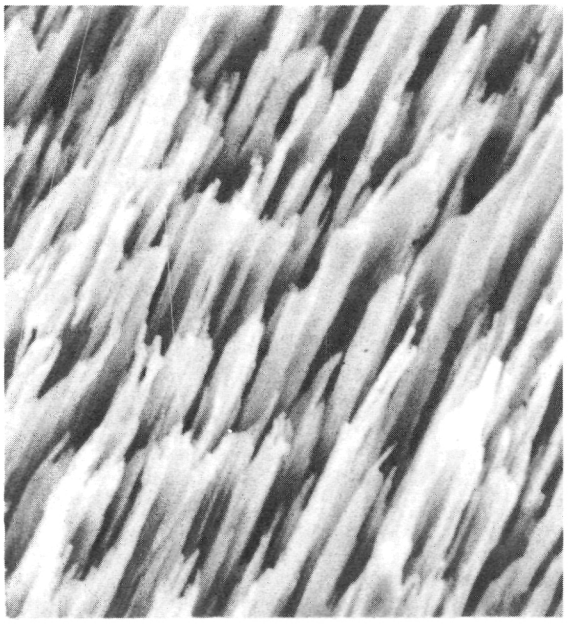

(c) Cones etched in copper.

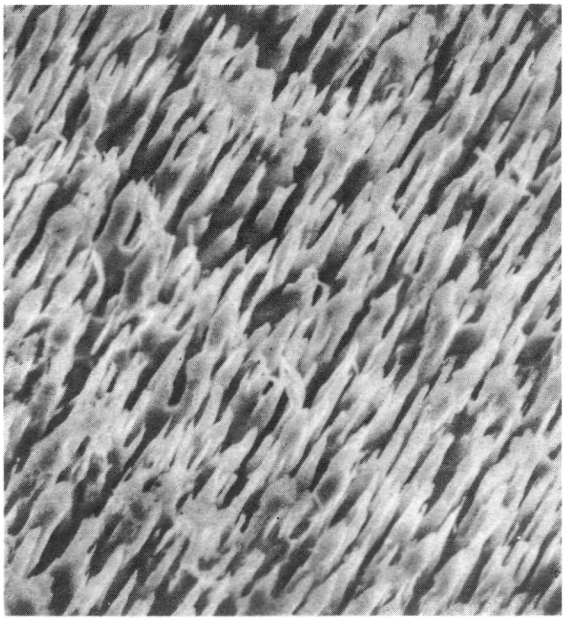

(d) Cones etched in gold.

Figure 32. - Scanning electron microscope photograph of etched cones. ×3000.

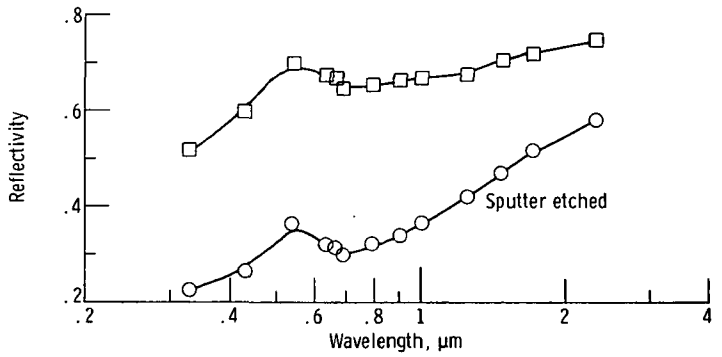

Figure 33. - Reflectivity of stainless steel (with and without sputter etch).

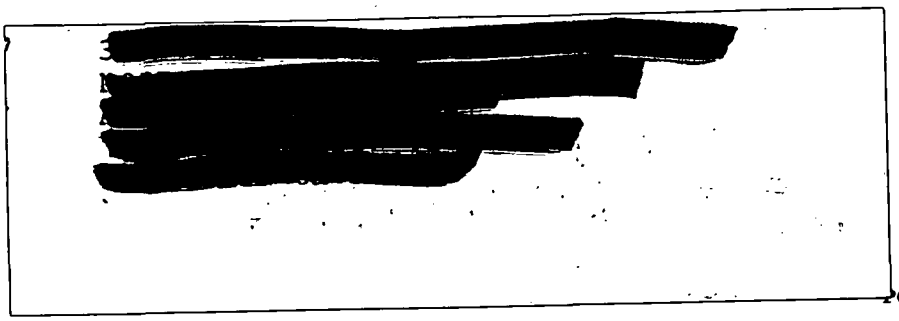

"The aeronautical and space activities of the United States shall be conducted so as to contribute . . . to the expansion of human knowledge of phenomena in the atmosphere and space. The Administration shall provide for the widest practicable and appropriate dissemination of information concerning its activities and the results thereof."

—NATIONAL AERONAUTICS AND SPACE ACT OF 1958

NASA SCIENTIFIC AND TECHNICAL PUBLICATIONS

TECHNICAL REPORTS: Scientific and technical information considered important, complete, and a lasting contribution to existing knowledge.

TECHNICAL NOTES: Information less broad in scope but nevertheless of importance as a contribution to existing knowledge.

TECHNICAL MEMORANDUMS: Information receiving limited distribution because of preliminary data, security classification, or other reasons. Also includes conference proceedings with either limited or unlimited distribution.

CONTRACTOR REPORTS: Scientific and technical information generated under a NASA contract or grant and considered an important contribution to existing knowledge.

TECHNICAL TRANSLATIONS: Information published in a foreign language considered to merit NASA distribution in English.

SPECIAL PUBLICATIONS: Information derived from or of value to NASA activities. Publications include final reports of major projects, monographs, data compilations, handbooks, sourcebooks, and special bibliographies.

TECHNOLOGY UTILIZATION PUBLICATIONS: Information on technology used by NASA that may be of particular interest in commercial and other non-aerospace applications. Publications include Tech Briefs, Technology Utilization Reports and Technology Surveys.

Details on the availability of these publications may be obtained from:

SCIENTIFIC AND TECHNICAL INFORMATION OFFICE

NATIONAL AERONAUTICS AND SPACE ADMINISTRATION

Washington, D.C. 20546